

Analysis of Spread Spectrum Time Domain Reflectometry for Wire Fault Location

Paul Smith, *Member, IEEE*, Cynthia Furse, *Senior Member, IEEE*, and Jacob Gunther, *Member, IEEE*

Abstract—Spread spectrum time domain reflectometry (SSTDR) and sequence time domain reflectometry have been demonstrated to be effective technologies for locating intermittent faults on aircraft wires carrying typical signals in flight. This paper examines the parameters that control the accuracy, latency, and signal to noise ratio for these methods. Both test methods are shown to be effective for wires carrying AC power signals, and SSTDR is shown to be particularly effective at testing wires carrying digital signals such as Mil-Std 1553 data. Results are demonstrated for both controlled and uncontrolled impedance cables. The low test signal levels and high noise immunity of these test methods make them well suited to test for intermittent wiring failures such as open circuits, short circuits, and arcs on cables in aircraft in flight.

Index Terms—Aging wire detection, arc detection, sequence time domain reflectometry (STDR), spread spectrum time domain reflectometry (SSTDR), time domain reflectometry (TDR), wire fault detection.

I. INTRODUCTION

FOR MANY years, wiring has been treated as a system that could be installed and expected to work for the life of an aircraft [1]. As aircraft age far beyond their original expected life span, this attitude is rapidly changing. Aircraft wiring problems have recently been identified as the likely cause of several tragic mishaps [2] and hundreds of thousands of lost mission hours [3]. Modern commercial aircraft typically have more than 100 km of wire [2]. Much of this wire is routed behind panels or wrapped in special protective jackets, and is not accessible even during heavy maintenance when most of the panels are removed.

Among the most difficult wiring problems to resolve are those that involve intermittent faults [4]. Vibration that causes wires with breached insulation to touch each other or the airframe, pins, splices, or corroded connections to pull loose, or “wet arc faults” where water drips on wires with breached insulation causing intermittent line loads. Once on the ground these faults

often cannot be replicated or located. During the few milliseconds it is active, the intermittent fault is a significant impedance mismatch that can be detected, rather than the tiny mismatch observed when it is inactive. A wire testing method that could test the wires continually, including while the plane is in flight would, therefore, have a tremendous advantage over conventional static test methods.

Another important reason to test wires that are live and in flight is to enable arc fault circuit breaker technology [5] that is being developed to reduce the danger of fire due to intermittent short circuits. Unlike traditional thermal circuit breakers, these new circuit breakers trip on noise caused by arcs rather than requiring large currents. The problem is that locating the tiny fault after the breaker has tripped is extremely difficult, perhaps impossible. Locating the fault before the breaker trips could enable maintenance action.

This paper describes and analyzes one such method, based on spread spectrum communication techniques that can do just that. This method is accurate to within a few centimeters for wires carrying 400-Hz aircraft signals as well as MilStd 1553 data bus signals. Results are presented on both controlled and uncontrolled impedance cables up to 23 m long.

Early research on spread spectrum time domain reflectometry (SSTDR) [6] has considered fault location tests on high voltage power wires. Sequence time domain reflectometry (STDR) [7] has been studied and used to test twisted pairs for use in communications. More recently, it has been demonstrated for location of intermittent faults such as those on aircraft wiring [18]. These test methods could be used as part of a smart wiring system [2], and could provide continuous testing of wires on aircraft in flight, with automatic reporting of fault locations to facilitate quick wiring repairs. This could be done by integrating the electronics into either the circuit breaker or into “connector savers” throughout the system. In order for this to be feasible, the prototype system that has been described here is being redesigned as a custom ASIC, which should cost on the order of \$10–\$20 per unit in bulk. This paper focuses on the analysis of SSTDR and STDR. Parameters required for these methods to function as potential test methods on wires carrying 400-Hz AC or high speed digital data such as Mil-Std 1553 are discussed. This analysis is critical to determine the system tradeoffs between speed, accuracy, code length/system complexity, etc. This ideal analysis provides information on the expected accuracy, which is verified with tests of near-ideal lossless controlled impedance coax. The effect of realistic noncontrolled impedance cable is also evaluated, and sources of error within a realistic system are discussed.

Manuscript received April 10, 2004; revised September 14, 2004. This work was supported in part by the Utah Center of Excellence for Smart Sensors and in part by the National Science Foundation under Contract 0097490. The associate editor coordinating the review of this paper and approving it for publication was Prof. Michael Pishko.

P. Smith is with VP Technology, LiveWire Test Labs., Inc., Salt Lake City, UT 84117 USA (e-mail: psmith@livewiretest.com).

C. Furse is with the Department of Electrical and Computer Engineering, University of Utah, Salt Lake City, UT 84112 USA, and also with VP Technology, LiveWire Test Labs., Inc., Salt Lake City, UT 84117 USA (e-mail: cfurse@ece.utah.edu).

J. Gunther is with the Department of Electrical and Computer Engineering, Utah State University, Logan, UT 84322-4120 USA (e-mail: jake@ece.usu.edu).

Digital Object Identifier 10.1109/JSEN.2005.858964

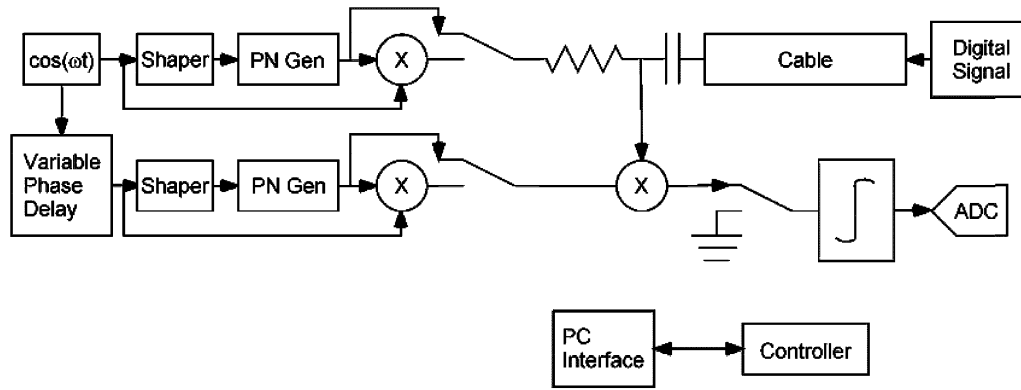


Fig. 1. S/SSTDR circuit diagram.

II. CURRENT WIRE TEST TECHNOLOGY

There are several test technologies that can be used to pinpoint the location of wiring faults. Some of the most publicized methods are: time domain reflectometry (TDR) [8], standing wave reflectometry (SWR) [12], frequency domain reflectometry (FDR) [13], impedance spectroscopy [14], high voltage, inert gas [15], resistance measurements, and capacitance measurements. At the present time, these test methods cannot reliably distinguish small faults such as intermittent failures on noncontrolled impedance cables without the use of high voltage. In addition, the signal levels required to reliably perform these tests may interfere with aircraft operation if applied while the aircraft is in use [4]. Another test method is needed that can test in the noisy environment of aircraft wiring, and that can be used to pinpoint the location of intermittent faults such as momentary open circuits, short circuits, and arcs.

III. SPREAD SPECTRUM WIRE TESTING

Spread spectrum signals, both in baseband (STDR) [7] and modulated (SSTDR) [6], are detectable through cross correlation, even though they may be buried in noise. The ability to pick out the signal is due to processing gain, which for direct sequence spread spectrum (DSSS) can be expressed as

$$PG = \frac{T_s}{T_c} = \frac{R_c}{R_s} = \frac{W_{ss}}{2R_s}$$

where W_{ss} is the bandwidth of the spread-spectrum signal, T_s is the duration of one entire STDR/SSTDR sequence (considering the entire sequence equal to one bit in communication-system terms), T_c is the duration of a PN code chip, R_c is the chip rate in chips per second, and R_s is the symbol rate, which in this case is the number of full sequences per second [16].

Because of this processing gain, it is reasonable to assume that a spread spectrum test system could operate correctly in a noisy environment with 400-Hz 115-V AC or digital data on the wires. The test system could be designed such that it would not be damaged by or interfere with any of the signals already on the wires. For the analysis that follows, the digital data on the wires will be assumed to be Mil-Std 1553, a standard aircraft communication data bus that specifies a 1 Mbit/second data rate, a 2.25–20 V RMS signal level, normally operates on low-loss

(3 dB/100 m) 70- Ω shielded twisted pair cable, and allows for a SNR of 17.5 dB [17].

The block diagram of the STDR/SSTDR block is shown in Fig. 1. A sine wave generator (operating at 30–100 MHz) creates the master system clock. Its output is converted to a square wave via a shaper, and the resulting square wave drives a pseudo-noise digital sequence generator (PN Gen). To use SSTDR, the sine wave is multiplied by the output of the PN generator, generating a DSSS binary phase shift keyed (BPSK) signal. To use STDR, the output of the PN generator is not mixed with the sine wave. The test signal is injected into the cable. The total signal from the cable (including any digital data or AC signals on the cable, and any reflections observable at the receiver) is fed into a correlator circuit along with a reference signal. The received signal and the reference signal are multiplied, and the result is fed to an integrator. The output of the integrator is sampled with an analog-to-digital converter (ADC). A full correlation can be collected by repeatedly adjusting the phase offset between the two signal branches and sampling the correlator output. The location of the various peaks in the full correlation indicates the location of impedance discontinuities such as open circuits, short circuits, and arcs (intermittent shorts). Test data indicate that this test method can resolve faults in a noisy environment to within 1/10th to 1/100th the length of a PN code chip on the cable, depending on the noise level, cable length, and type of cable [4].

IV. STDR/SSTDR ANALYSIS

The operation of STDR/SSTDR depends on the fact that portions of electrical signals are reflected at discontinuities in the characteristic impedance of the cable. A spread spectrum signal shown in Fig. 2 is injected onto the wires, and as with TDR, the reflected signal will be inverted for a short circuit and will be right-side-up for an open circuit [8]. The observed reflected signal is correlated with a copy of the injected signal. The shape of the correlation peaks is shown in Fig. 3. In this figure, the modulating frequency is the same as the chip rate. Note that the sidelobes in the correlation peak are sinusoids of the same amplitude as the off-peak autocorrelation of the ML code. This is due to the selected modulation frequency and synchronization. Use of a different modulation frequency or different synchronization will yield a different correlation pattern that may have higher side lobes [4]. Different PN sequences also have different peak shapes, as shown in Fig. 4 for ML and gold codes.

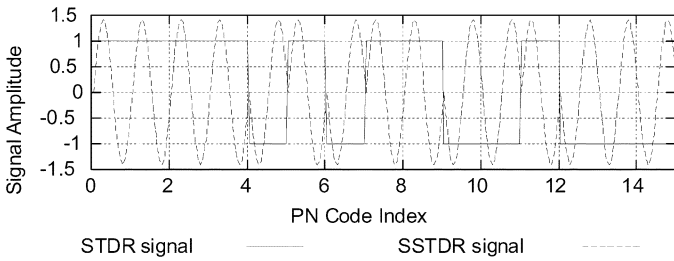


Fig. 2. STDR and SSTDR signals. The SSTDR signal is modulated with $1.0 \cdot F_{\text{STDR}}$.

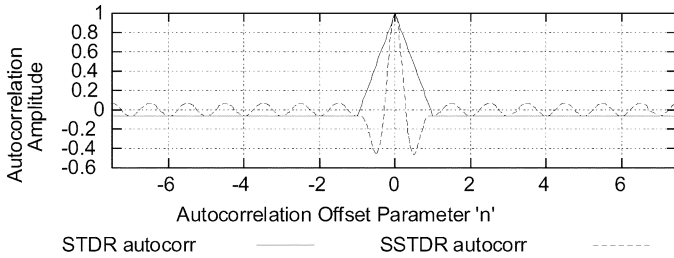


Fig. 3. Autocorrelations of STDR and SSTDR signals from Fig. 2.

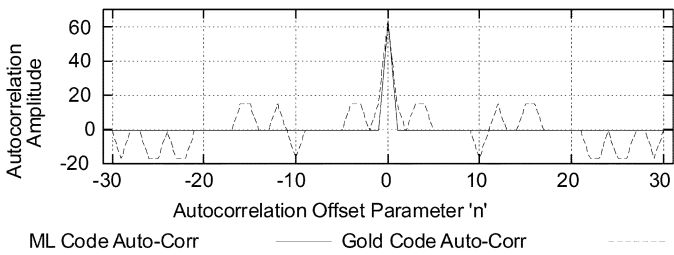


Fig. 4. Autocorrelations of ML and gold codes.

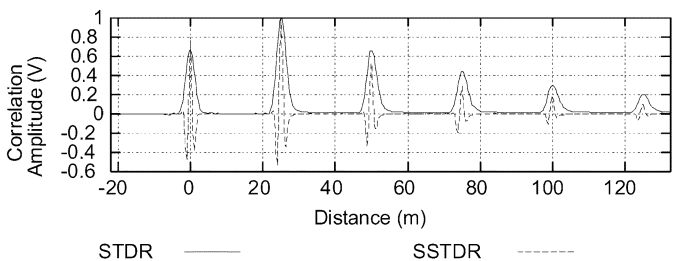


Fig. 5. Correlator output for STDR and SSTDR tests on $75\text{-}\Omega$ coax cable with an open circuit 23 m down the cable. Note the peak at zero (connection between the test system and cable), multiple reflections, and definitive shape of the correlation peaks.

The location of the peaks in the correlator output in conjunction with an estimate of the velocity of propagation indicates the distance to impedance discontinuities. Fig. 5 shows normalized sample test data collected on $75\text{-}\Omega$ coax cable. The correlation peaks after 23 m are due to multiple reflections in the 23-m cable. The response for noncontrolled impedance cable is not as clean, which is to be expected because of the variation in impedance and subsequent small reflections as well as minor variation in velocity of propagation down the length of the cable. Fig. 6(a) and (b) show the STDR and SSTDR correlation responses measured on two 22 AWG wires in a loosely bundled set of 22 wires that is 9.9 m long. The wires snake in and out within the bundle, and although they are roughly parallel

throughout, they definitely do not have even spacing throughout the bundle. The response is not as smooth as that seen in Fig. 5, due to the multiple small reflections that occur within the uncontrolled impedance bundle. These multiple reflections as well as the variations in velocity of propagation that go with them will reduce the accuracy of the method somewhat for uncontrolled impedance cables, as we shall see later.

When a peak detection algorithm (to identify the approximate open circuit location) is coupled with a curve fitting approach (to determine its precise location), the length of the wires can be calculated very accurately as shown in Fig. 4(a) and (b) for the controlled and uncontrolled impedance wires, respectively. The maximum error observed for controlled impedance cables is 3 cm, and for the uncontrolled impedance wires is 6 cm. The minimum measurable length for both systems is approximately 3.5 m, as seen in these figures. This is because the initial and final peaks overlap. A more advanced curve fitting approach can be used to distinguish these overlapping peaks.

For the discussion that follows, the ideal case will be assumed where the cable is lossless. An additional assumption is that frequency dispersion is negligible in the cable. That is, that all frequencies travel down the cable at the same rate.

A. Expected Correlator Output With Generalized Noise

The correlator output can be analyzed in terms of the signal injected onto the cable, various reflections of that signal, and any unwanted signals (noise) received at the correlator input.

Let $S[n]$ be a recursive linear sequence of period K consisting of 1s and -1 s. Then let

$$s(t) = \sum_{n=-\infty}^{\infty} S[n] \cdot p(t - nT) \quad (1)$$

where

$$p(t) = \begin{cases} 1, & 0 \leq t \leq T_c \\ 0, & \text{otherwise} \end{cases} \quad (2)$$

so that $s(t)$ is a recursive linear signal (RLS) of period $T_s = KT_c$ consisting of 1s and -1 s. Here, T_c is the minimum duration of a 1 or -1 , otherwise known as a ‘‘chip.’’ Note that

$$s(t) = s(t + T_s) \quad (3)$$

for any t for a RLS of duration T_s .

The test system will send a signal $s(t)$ onto the cable, which will be reflected by some arbitrary number of impedance discontinuities in the cable. The reflected signals will return to the test system after some transmission delay. Along with the reflected signals will be some noise that will depend on the nature of the cable being tested, anomalies in the signal generation, and extraneous noise. The noise could be white noise, or it could contain signals such as Mil-Std 1553.

Let $x(t)$ be the received signal, defined as

$$x(t) = \sum_k a_k s(t - \tau_k) + n(t) \quad (4)$$

where a_k is the amplitude of reflected signal $a_k s(t - \tau_k)$ relative to $s(t)$, τ_k is the time delay before receiving reflection k , and

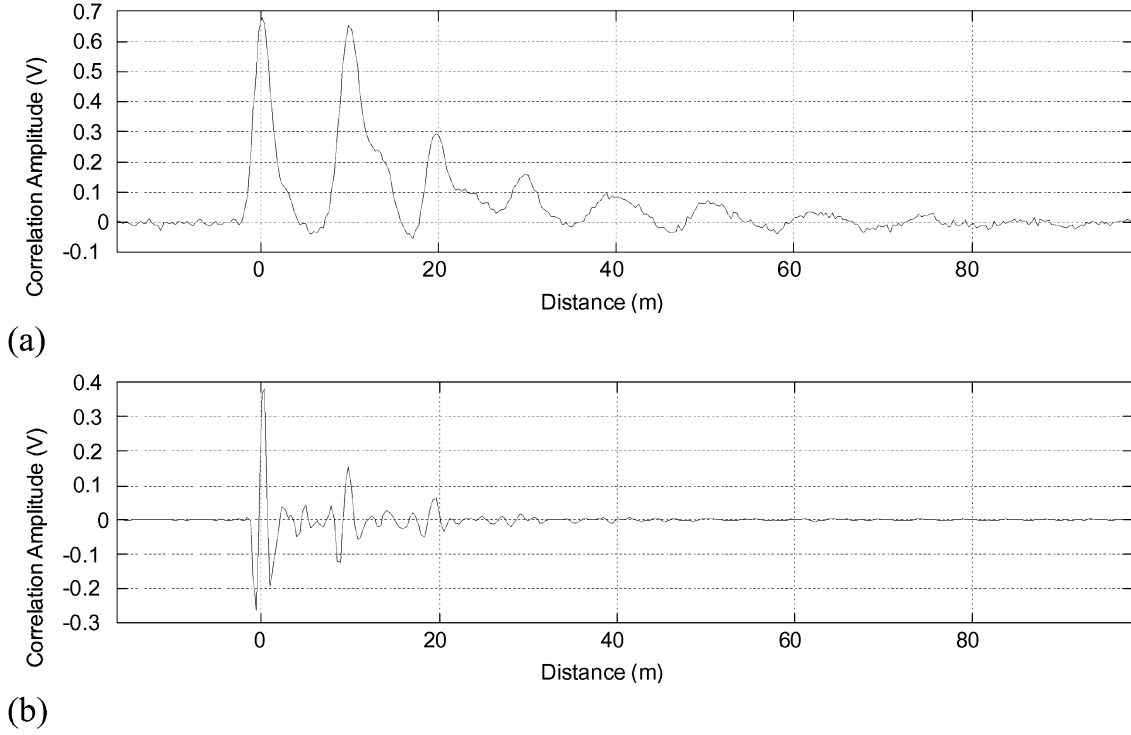


Fig. 6. (a) STDR and (b) SSTDR correlation response for an open circuit measured on two 22 AWG wires in a loosely bundled set of 22 wires that is 9.9 m long.

$n(t)$ is a noise signal of duration $T_n \gg T_s$, that is statistically uncorrelated to $s(t)$.

The correlator output will be

$$\begin{aligned}
 R_{sx\tau} &= \int_0^{T_s} s(t)x(t-\tau) dt \\
 &= \int_0^{T_s} s(t) \sum_k a_x s(t-\tau-\tau_k) dt \\
 &\quad + \int_0^{T_s} s(t)n(t-\tau) dt.
 \end{aligned} \quad (5)$$

As can be seen from (5), the correlator output will depend on the reflected signals and the noise, and is, therefore, determined by both deterministic and nondeterministic signals. The expected value $E(\cdot)$ of the correlation $R_{sx\tau}$ must, therefore, be considered

$$\begin{aligned}
 E\{R_{sx\tau}\} &= E \left\{ \int_0^{T_s} s(t) \sum_k a_x s(t-\tau-\tau_k) dt \right. \\
 &\quad \left. + \int_0^{T_s} s(t)n(t-\tau) dt \right\} \\
 &= \int_0^{T_s} s(t) \sum_k a_x s(t-\tau-\tau_k) dt.
 \end{aligned} \quad (6)$$

In the last step in (6), the fact that $s(t)$ is zero mean and $n(t)$ is asynchronous to $s(t)$ was used.

The output of the correlator in the absence of noise is the sum of cross correlations of scaled and time-shifted copies of $s(t)$ and the original $s(t)$. The expected output in the presence of noise is the same as the output in the absence of noise, with some additional random noise term that is zero mean.

B. Correlator Output in the Presence of White Noise

The cross correlation of noise terms with $s(t)$ can be discussed in terms of the nature of the noise terms. If $n(t)$ is white Gaussian noise, the cross-correlation analysis can be described explicitly [11]. From (6), the cross correlation of $s(t)$ with $n(t)$ has mean

$$E\{R_{sn\tau}\} = E \left\{ \int_0^{T_s} s(t)n(t-\tau) dt \right\} = 0 \quad (7)$$

and variance

$$E\{R_{sn\tau}^2\} = \frac{N_0}{2} E_s \quad (8)$$

where $N_0/2$ is the noise power received at the input, and E_s is the energy in the reference signal $s(t)$ over one period.

Thus, the effect of white noise in the system will be to add variation to the measurements proportional to the energy of the signal $s(t)$, but it will not cause a consistent DC offset.

C. Correlator Output in the Presence of Mil-Std 1553

As with white noise, the mean output of the correlator with Mil-Std 1553 as the noise source $n(t)$ is zero as shown in (6). The variance of the noise is a bit more involved to calculate since for Mil-Std 1553

$$E\{n(t_1-\tau)n(t_2-\tau)\} \text{ not proportional to } \delta(t_1-t_2) \quad (9)$$

which is not the same as it is for white noise, as shown in (8).

The signal used for correlation $s(t)$ will be integrated over a single period. It can, therefore, be considered to be an energy signal [11], and its energy spectral density is given by

$$G_{s(f)} = |F\{s(t)\}|^2 = |S(f)|^2 \quad (10)$$

where $S(f)$ is the Fourier transform of $s(t)$. Since $s(t)$ is of finite duration, its power spectral density (PSD) is only nonzero if considered only over the integration time T_s , in which case

$$\text{PSD}_s(f) = \frac{|S(f)|^2}{T_s}. \quad (11)$$

The total energy in the signal $s(t)$ can be found in several ways as given by Rayleigh's theorem [11]

$$\begin{aligned} E_s &= \int_0^{T_s} s^2(t) dt = \int_{-\infty}^{\infty} |S(f)|^2 df \\ &= T_s \int_{-\infty}^{\infty} \text{PSD}_s(f) df. \end{aligned} \quad (12)$$

Let $n(t)$ be the noise signal due to Mil-Std 1553 operating on the wires. The Fourier transform of $n(t)$ is given by

$$N(f) = \int_{-\infty}^{\infty} n(t)e^{-j2\pi ft} dt. \quad (13)$$

Rayleigh's theorem gives the energy of the signal $n(t)$ as

$$\begin{aligned} E_n &= \int_{\kappa}^{\kappa+T_n} n^2(t) dt = \int_{-\infty}^{\infty} |N(f)|^2 df \\ &= T_n \int_{-\infty}^{\infty} \text{PSD}_n(f) df \end{aligned} \quad (14)$$

and the PSD defined over T_n as

$$\text{PSD}_n(f) = \frac{|N(f)|^2}{T_n}. \quad (15)$$

As $n(t)$ is not a periodic function, the cross-correlation functions listed below that deal with $n(t)$ will be linear cross correlations. If both $s(t)$ and $n(t)$ or their derivatives are used in a cross correlation, it will be operating on one cycle of $s(t)$ and be defined over $0 \leq t \leq T_n$, unless otherwise specified. If only $s(t)$ is shown in a cross correlation or autocorrelation, it will be a circular cross correlation or autocorrelation, and will be nonzero only for $0 \leq t \leq T_s$. Since $T_n \gg T_s$, $T_n + T_s \approx T_n$, and will be treated as if $T_n + T_s = T_n$.

The Fourier transform of the cross correlation of $s(t)$ and $n(t)$ is

$$F\{R_{sn}(t)\} = F\{s(t) * n(-t)\} = S(f)N^*(f) \quad (16)$$

where $N^*(f)$ is the complex conjugate of $N(f)$.

The energy in this cross correlation is

$$E_{R_{sn}} = \int_{-\infty}^{\infty} |R_{sn}(t)|^2 dt = \int_{-\infty}^{\infty} |S(f)|^2 |N(f)|^2 df. \quad (17)$$

The expected energy in the cross correlation over time $0 \leq t \leq T_s$ is given by

$$\begin{aligned} E\{E_{R_{sn}, T_s}\} &= \frac{T_s}{T_n} E \left\{ \int_{-\infty}^{\infty} |S(f)|^2 |N_{T_s}(f)|^2 df \right\} \\ &= \frac{T_s}{T_n} \int_{-\infty}^{\infty} |S(f)|^2 |N(f)|^2 df \approx E_{R_{sn}, T_s} \end{aligned} \quad (18)$$

where $N_{T_s}(f)$ is the Fourier transform of the subsection of $n(t)$ used for the cross correlation for $0 \leq t \leq T_s$. Note that, in general, $N_{T_s}(f) \neq N(f)$ because the cross correlation may be over only a few bits of $n(t)$. However, the expected value for $N_{T_s}(f)$ is $N(f)$.

The expected noise power is

$$P_{R_{sn}} = \frac{E_{R_{sn}, T_s}}{T_s} = \frac{E_{R_{sn}}}{T_n} = \frac{\int_{-\infty}^{\infty} |S(f)|^2 |N(f)|^2 df}{T_n} \quad (19)$$

which is true for any noise source $n(t)$, including the Mil-Std 1553 signal.

It is clear that (19) indicates that spectral overlap between the noise and STDR/SSTDR signal results in unavoidable noise in the correlator output.

D. SSTDR Modulation

In order to perform a consistent cross correlation, a reference signal must be available. This brings us to the question of synchronization. If the reference signals modulation is off by 90° from the driving signals modulation, the cross correlation of the received signal and the reference signal would be zero, as the two signals would be orthogonal to each other. Another cross correlation of the same signal could return a different result, if the phase difference between the modulating frequency and the PN code changed. This would make the system very difficult to calibrate. Because the choice has been made to use PN codes, it makes sense to synchronize the modulating sinewave with the PN code [4]. By generating the signals in a consistent way, a reference signal can be generated which can be used consistently with the injected signal, providing for a system that gives consistent results under similar circumstances.

Sample aircraft cables tested with S/SSTDR have significant loss at high frequency. Noncontrolled impedance cables (discrete bundled wires) over 60 m long have been tested with STDR and over 15-m long have been tested with SSTDR (which has higher frequency content).

Another effect of realistic aircraft cable is the effect of variation in the velocity of propagation (VOP). Typical wires have VOP ranging from 0.66 to 0.76 times the speed of light [9]. If the type of wire is known, the correct velocity can be used to obtain the best possible calculation for the length of the wire. If the type of wire is not known, and average values are used, additional errors of up to 10% could be observed. Correlation peaks show higher dispersion if they are due to reflections farther down the cable, as shown in Fig. 2. This effect can be accounted for by changing the shape that is matched by the curve fitting algorithm as it is applied to reflections from different lengths down the cable.

Results for both controlled and uncontrolled impedance aircraft cables with a variety of signals on the line were tested [4]. Using curve fitting, both methods had errors on the order of 3 cm for controlled impedance coax and 6 cm for uncontrolled bundled cable with or without 60-Hz signals for both open and short circuited cables. However, as expected, SSTDR performs significantly better than STDR in the presence of the MilStd-1553 signal utilizing the uncontrolled impedance bundled wire (a worse case than normal, since MilStd 1553 would

normally be implemented on controlled impedance twisted pair wire). For an SNR of -24 dB, STDR has an error of about 24 cm, and SSTDR had less than 3 cm of error. SSTDR still had less than 6 cm of error down to and SNR of -53 dB below the MilStd 1553 data signal. Both methods could be used effectively, since the required SNR for MilStd 1553 is -17 dB, however the advantage of SSTDR for a high frequency noisy environment was clearly demonstrated.

V. SIGNAL-TO-NOISE RATIO

The SNR is defined as the signal power divided by the average noise power. For a digital signal such as Mil-Std 1553, this would be expressed as

$$\frac{S}{N} = \frac{\text{Mil Std 1553 Power}}{\text{Background Noise Power}}. \quad (20)$$

In the case of STDR/SSTDR, the STDR and SSTDR signals are the desired signals, and other signals are noise. Therefore, considering the signal-to-noise power of the STDR and SSTDR signals in the presence of another signal (Mil-Std 1553 in this example), gives

$$\frac{S}{N} = \frac{\text{XCORR(STDR or SSTDR Signal)}}{\text{XCORR(Mil) Std 1553 + Background Noise}} \quad (21)$$

after correlation, where $\text{XCORR}(\cdot)$ means ‘‘cross-correlated power.’’

The reflection terms $g_k = a_k s(t - \tau_k)$ represent the reflections at various distances down the cable. To detect each of these signals, the correlator offset is set to time $t = \tau_k$. All other reflection terms are considered noise terms. The received signal after cross correlation is

$$R_{sgk}(t_k) = a_k E_s. \quad (22)$$

From (22) and (19), the SNR is

$$\left(\frac{S}{N}\right) = \frac{a_k^2 E_s^2}{\int_{-\infty}^{\infty} |S(f)X(f)|^2 df} = \frac{a_k^2 E_s^2 T_s}{\int_{-\infty}^{\infty} |S(f)X(f)|^2 df}. \quad (23)$$

The integral in (23) needs to be carried out for every signal of interest that could be a noise source. For spectrally narrow noise, such as the 115 V 400 Hz on aircraft, (23) simplifies to

$$\begin{aligned} \left(\frac{S}{N}\right) &= \frac{a_k^2 E_s^2 T_s}{\int_{-\infty}^{\infty} |S(f)X(f)|^2 df} \\ &= \frac{a_k^2 E_s^2 T_s}{\int_{-\infty}^{\infty} \left|S(f)\sqrt{2} \frac{\delta(f-400 \text{ Hz}) + \delta(f+400 \text{ Hz})}{2}\right|^2 df} \\ &= \frac{\sqrt{2}}{115} \frac{a_k^2 E_s^2 T_s}{(|S(400 \text{ Hz})|^2 + |S(-400 \text{ Hz})|^2)}. \end{aligned} \quad (24)$$

From this, it can be seen that if $S(f)$ has very little of its energy centered at ± 400 Hz, the SNR will be large.

For noise signals that are broad in frequency spectrum, the integral in (23) is quite involved, and is best handled numerically on a case-by-case basis.

The effects of changing certain parameters can be studied analytically in such a way as to provide excellent insight into factors other than signal and noise power that affect the SNR. These analyzes are carried out below.

A. Changing the Length of the STDR/SSTDR Signal

In order to approximate a signal with m times the number of chips as $s(t)$, let us define a new signal $s_m(t)$ such that $|S_m(f)|$ is proportional to $|S(f)|$, and let the duration of $s_m(t)$ be $mT_s = T_{sm}$. Letting the amplitude of $s_m(t)$ be the same as $s(t)$

$$E_{s_m} = \int_{-\infty}^{\infty} |s_m(t)|^2 dt = m \int_0^{T_s} |s(t)|^2 dt = mE_s. \quad (25)$$

In the frequency domain

$$\begin{aligned} E_{s_m} &= \int_{-\infty}^{\infty} |S_m(f)|^2 df = \int_{-\infty}^{\infty} |\sqrt{m}S(f)|^2 df \\ &\therefore |S_m(f)| = |\sqrt{m}S(f)| \end{aligned} \quad (26)$$

which is what would be expected if the duration of $s(t)$ were increased by a factor of m by adding more chips to its sequence.

Letting

$$R_{s_m n}(t) = s_m(t) * n(-t) \quad (27)$$

gives

$$E_{R_{s_m n}} = \int_{-\infty}^{\infty} |S_m(f)|^2 |N(f)|^2 df = mE_{R_{sn}} \quad (28)$$

which is the noise energy in the cross correlation of $s(t)$ with $n(t)$ over the time $0 \leq t \leq T_n$. The expected value of the noise power over the interval $0 \leq t \leq T_s$ is the noise power over the interval $0 \leq t \leq T_n$, given by

$$P_{R_{s_m n}} = \frac{E_{R_{s_m n}}}{T_n} = \frac{mE_{R_{sn}}}{T_n} = mP_{R_{sn}} \quad (29)$$

which is valid because $T_n \gg T_s$.

The central peak of the autocorrelation is given by

$$R_{s_m}(0) = E_{s_m} = mE_s. \quad (30)$$

The signal power is

$$(R_{s_m}(0))^2 = (mE_s)^2 = m^2 E_s^2. \quad (31)$$

From (31) and (29), the SNR is

$$\left(\frac{S}{N}\right)_m = \frac{m^2 E_s^2}{mP_{R_{sn}}} = m \frac{E_s^2}{P_{R_{sn}}} = m \left(\frac{S}{N}\right). \quad (32)$$

Equation (32) shows that doubling the length of the PN code while leaving all other parameters the same will double (increase by 3 dB) the SNR. This is true for any noise type including 400-Hz ac, Mil-Std 1553, and white noise.

B. Scaling the Frequency of the STDR/SSTDR Signal

Let $s_\psi(t) = s(\psi t)$, and $T_{s_\psi} = (T_s/\psi)$, where ψ is a constant. Using the scaling property of the Fourier transform and assuming $\psi \geq 1$

$$S_\psi(f) = \frac{1}{|\psi|} S\left(\frac{f}{\psi}\right) = \frac{1}{\psi} S\left(\frac{f}{\psi}\right). \quad (33)$$

The signal of interest after correlation is the peak value in the autocorrelation of $s_\psi(t)$, which is $R_{s_\psi}(0)$, and corresponds to the energy in $s_\psi(t)$, given by

$$R_{s_\psi}(0) = \int_0^{T_{s_\psi}} |s(\psi t)|^2 dt = \frac{1}{\psi} E_s. \quad (34)$$

Examining correlator noise output, we have

$$R_{s_\psi n}(t) = s_\psi(t) * n(-t) \quad (35)$$

and

$$E_{R_{s_\psi n}} = \frac{1}{\psi^2} \int_{-\infty}^{\infty} \left| S\left(\frac{f}{\psi}\right) \right|^2 |N(f)|^2 df. \quad (36)$$

If STDR is considered with the chip rate much greater than the Mil-Std 1553 data rate of 1 MHz, it can be assumed that $S(f)$ is approximately constant in the region where the majority of the power of $N(f)$ exists. Then, $(1/\psi)S(f/\psi)$ will also be approximately constant in that region if $\psi \geq 1$. With these assumptions, (36) can be written as

$$E_{R_{s_\psi n}} \approx \int_{-\infty}^{\infty} |S(f)|^2 |N(f)|^2 df = \frac{1}{\psi^2} E_{R_{sn}} \quad (37)$$

and the average noise power is

$$P_{R_{s_\psi n}} = \frac{E_{R_{s_\psi n}}}{T_n} \approx \frac{\frac{1}{\psi^2} E_{R_{sn}}}{T_n} = \frac{1}{\psi^2} P_{R_{sn}}. \quad (38)$$

The SNR from (38) and (34) is

$$\left(\frac{S}{N}\right)_\psi \approx \frac{\frac{1}{\psi^2} E_s^2}{\frac{1}{\psi^2} P_{R_{sn}}} = \frac{E_s^2}{P_{R_{sn}}} = \left(\frac{S}{N}\right). \quad (39)$$

Equation (39) states that in STDR mode, doubling the chip rate of the PN code while leaving all other parameters the same will have no appreciable effect on the SNR for STDR tests if the major noise contributor is Mil-Std 1553.

Attention is now turned to changing the chip rate and modulation frequency for SSTDR tests. For SSTDR with a chip rate much greater than the Mil-Std 1553 data rate of 1 MHz, scaling the SSTDR chip rate and modulation frequency by a factor ψ will change the slope near $f = 0$ by a factor $1/\psi$. So, in the region where the Mil-Std 1553 signal is significant

$$\left| S\left(\frac{f}{\psi}\right) \right| \approx \frac{1}{\psi} |S(f)|. \quad (40)$$

With this approximation

$$E_{R_{s_\psi n}} = \int_{-\infty}^{\infty} |S_\psi(f)|^2 |N(f)|^2 df = \frac{1}{\psi^4} E_{R_{sn}} \quad (41)$$

and the average noise power is

$$P_{R_{s_\psi n}} = \frac{E_{R_{s_\psi n}}}{T_n} \approx \frac{\frac{1}{\psi^4} E_{R_{sn}}}{T_n} = \frac{1}{\psi^4} P_{R_{sn}}. \quad (42)$$

The SNR from (42) and (34) is

$$\left(\frac{S}{N}\right)_\psi \approx \frac{\frac{1}{\psi^2} E_s^2}{\frac{1}{\psi^4} P_{R_{sn}}} = \psi^2 \left(\frac{S}{N}\right). \quad (43)$$

Equation (43) shows that in SSTDR mode, doubling the chip rate of the PN code and modulation frequency while leaving all other parameters the same will increase the SNR for SSTDR tests by 6 dB if the major noise contributor is Mil-Std 1553. This is vastly superior to the STDR results.

C. Self-Induced Noise

A certain amount of noise comes from the selection of a particular PN code. This is considered *noise*, because there is a deviation in the cross correlation of all PN codes from the ideal of a central peak with no side-lobes. Fig. 7 shows the autocorrelations of two identical-power PN sequences, one of which is using a ML code [10], and the other of which is using a gold code [10]. Note that the power in the two autocorrelations is not equal, even though the power in the signals used to generate them is equal. In fact, the power in the ML code autocorrelation is 56% the power in the gold code autocorrelation. This extra power in the gold code autocorrelation is self-induced noise power, and it reduces the SNR for STDR/SSTDR tests.

D. STDR/SSTDR Code Selection

The optimal PN code depends on the nature of the application. The PN code with the lowest side lobes in its autocorrelation is a ML code. It is, therefore, optimal for use when only one PN code will be used at a time.

The PN code with the next best autocorrelation properties is the Kasami code [11]. It is the best PN code choice when simultaneous tests on one or more conductors can interfere with each other. This is due to the high degree of orthogonality of signals in a Kasami set. If, however, the number of simultaneous tests exceeds the number of codes in the Kasami set, then codes with higher autocorrelation side-lobes, such as gold codes, may be used. One-shot codes, such as those similar to Barker codes, may also be used for STDR/SSTDR.

Many other PN codes are a poor choice for STDR/SSTDR due to high autocorrelation side lobes or the lack of a single autocorrelation peak.

E. STDR/SSTDR Using ML Codes

When the background noise is white noise, the total noise power after correlation is identical for both the STDR and SSTDR cases because the noise is spectrally flat. In this case, it is clear that there is little advantage of STDR over SSTDR or vice versa. However, when the noise is not spectrally flat, such as is the case with a Mil-Std 1553 or other digital data signal, the spectral overlap of the noise with the STDR/SSTDR signal will change the relative benefits of STDR versus SSTDR.

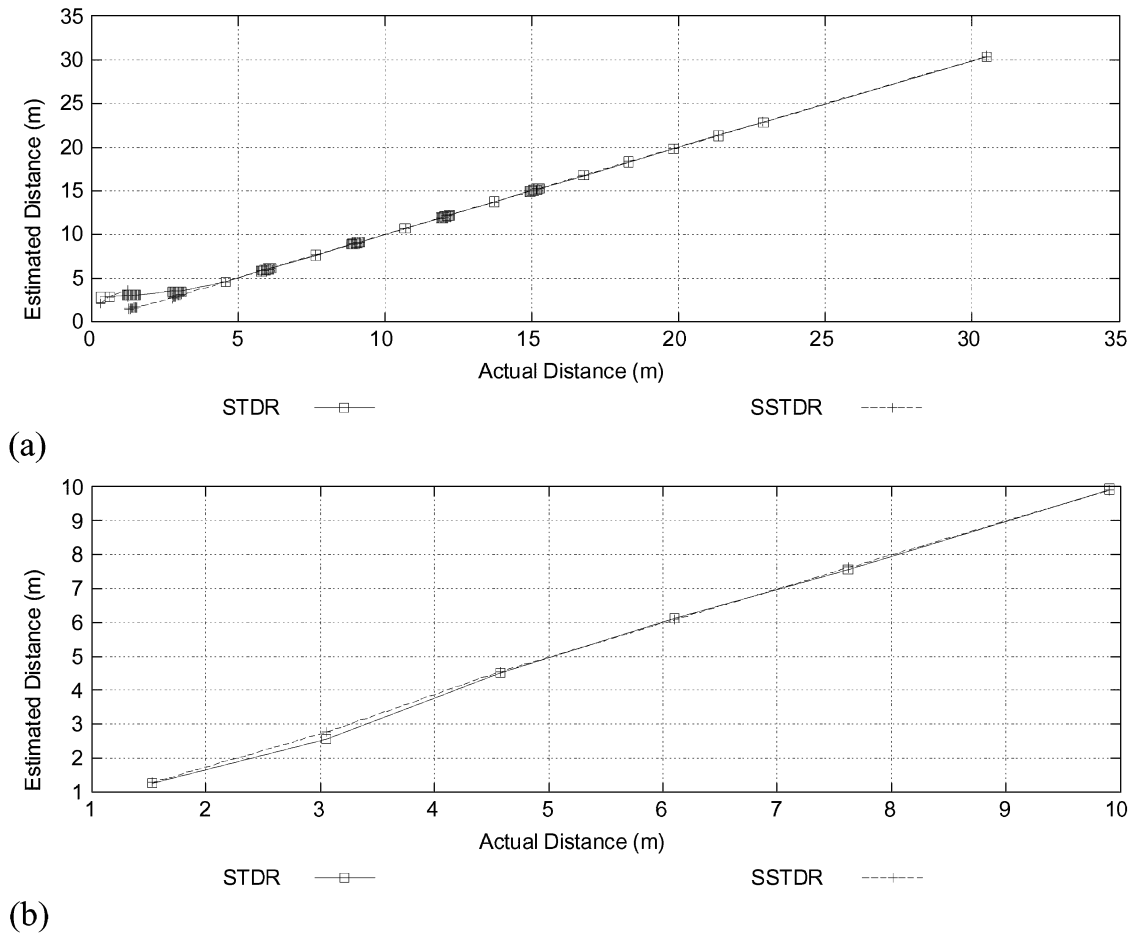


Fig. 7. Actual versus distance estimated with a curve-fit algorithm on (a) a 75-Ω cable and (b) a pair of two 22 AWG wires within a loose bundle of 22 wires tested with S/SSTDTR.

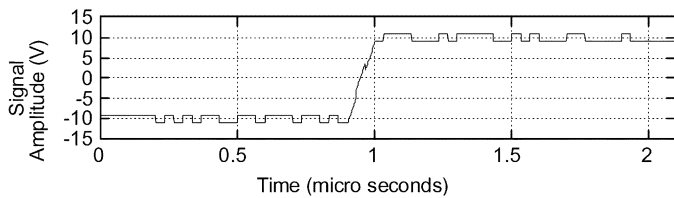


Fig. 8. ML code STDR signal at 1-V RMS, with a signal length of 63 chips at 30 MHz, operating in the presence of Mil-Std 1553 at 10-V RMS.

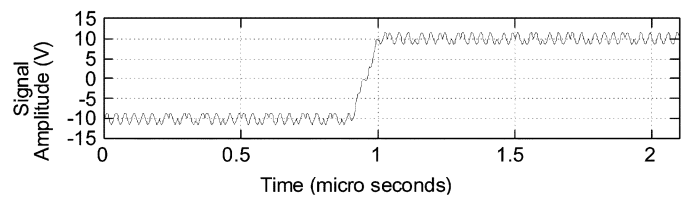


Fig. 9. ML code SSTDR signal at 1-V RMS, with a signal length of 63 chips at 30 MHz, operating in the presence of Mil-Std 1553 at 10-V RMS.

Fig. 8 shows a 1-V RMS STDR signal in the presence of 10-V RMS Mil-Std 1553. Since the Mil-Std 1553 signal is at 10-V RMS, it is 20 dB above the STDR signal level. The PN code length is 63 bits, which will give a processing gain of 36 dB. The chip rate in this figure is 30 MHz. The processing gain for longer STDR sequences is higher, so a lower power STDR signal can be used in an actual test system that will not interfere with the Mil-Std 1553 signal.

Fig. 9 shows a 1-V RMS SSTDR signal in the presence of 10-V RMS Mil-Std 1553. The PN code length used to generate this SSTDR signal is 63 bits.

Even after the 36 dB processing gain, the correlation peak shown in Fig. 10 is not clear due to the high noise level after correlation. Consider, however, the clarity of the correlation peak in Fig. 11. In both cases, the amplitude of the correlation peak

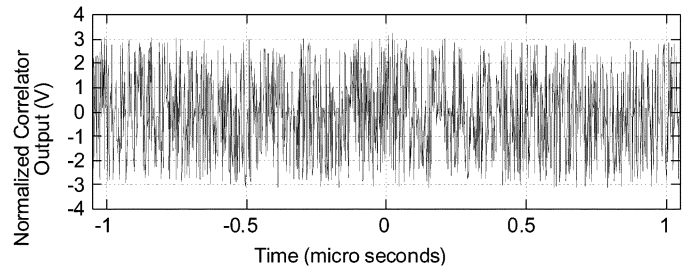


Fig. 10. Normalized cross correlation of a reference ML code STDR signal with the signal shown in Fig. 8.

is identical, but the background noise levels are significantly different.

To gain insights into the dramatic difference in background noise levels shown in Figs. 10 and 11, the spectral content of

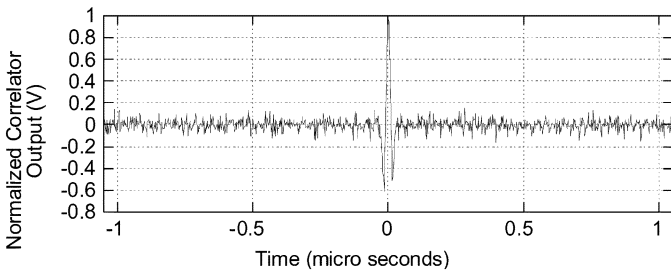


Fig. 11. Normalized cross correlation of a reference ML code SSTDR signal with the signal shown in Fig. 9.

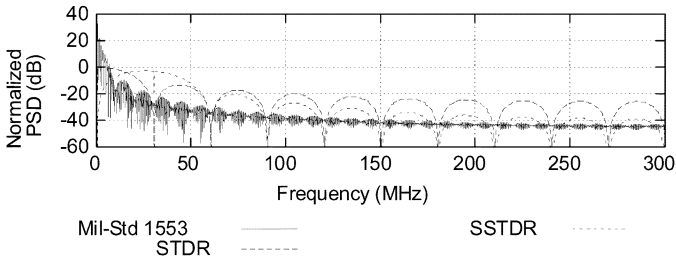


Fig. 12. Normalized PSD of a ML code STDR signal of length 63 chips at 30 MHz (1-V RMS), ML code SSTDR signal of length 63 chips at 30 MHz (1-V RMS), and Mil-Std 1553 (1-V RMS). Signals are normalized with respect to the peak STDR power.

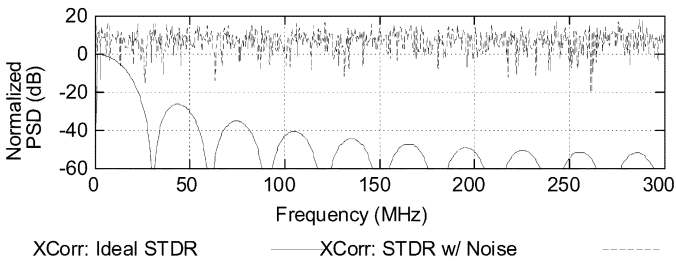


Fig. 13. Normalized PSD of the cross-correlator (XCorr) output for a pure ML code STDR (ideal case) signal of length 63 chips at 30 MHz (1-V RMS), and a 1-V RMS ML code STDR signal in the presence of a 10-V RMS Mil-Std 1553 signal.

the STDR and SSTDR signals with respect to the Mil-Std 1553 signal can be examined. The PSD of these three signals as used in the simulations is shown in Fig. 12, normalized to the peak STDR power.

In Fig. 12, it can be seen that the power in the Mil-Std 1553 signal is centered about 0 Hz, as is the power in the STDR signal. The SSTDR signal, however, slopes down to a spectral null at 0 Hz (dc). If this is considered in light of (19), it is clear that there will be significantly more unwanted power in the cross correlation of an STDR signal with Mil-Std 1553 than there will be in the cross correlation of an SSTDR signal with Mil-Std 1553.

To compare SSTDR with STDR, frequencies above the chip rate were not trimmed off prior to modulation, which caused some aliasing in the SSTDR case. Tests performed using bandlimiting prior to modulation did not show a significant difference in the SSTDR correlator output.

Fig. 13 shows the PSD of the cross correlation shown in Fig. 12, alongside the cross correlation of an STDR signal in the ideal case where there is no noise. The background noise completely dwarfs the desired signal. The frequency spectrum of the noise is broad due to the random sampling of the noise

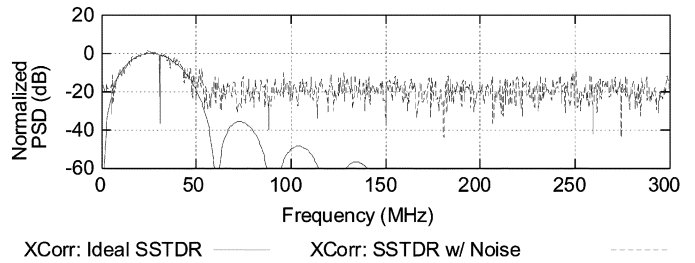


Fig. 14. Normalized PSD of the cross-correlator (XCorr) output for a pure ML code SSTDR (ideal case) signal of length 63 chips at 30 MHz (1-V RMS), and a 1-V RMS ML code SSTDR signal in the presence of a 10-V RMS Mil-Std 1553 signal.

that naturally occurs in a single sample per iteration correlator design.

Fig. 14 shows the PSD of the cross correlation shown in Fig. 11, alongside the cross correlation of an SSTDR signal in the ideal case where there is no noise. The background noise is significantly lower than the peak of the desired signal. Again, the frequency spectrum of the noise is broad due to the random sampling of the noise that naturally occurs in a single sample per iteration correlator design.

It is clear from these simulations that STDR and SSTDR can be used to find impedance changes in wiring. It is also clear that the spectral content of the SSTDR signal can be adjusted to avoid mutual interference between the SSTDR and digital signals on the wires. Tests with narrowband noise, such as 400-Hz 115-V ac, show a negligible effect on the correlator output compared to wideband noise such as the digital signals discussed above.

VI. CONCLUSION

This paper has examined STDR and SSTDR using ML codes. Equations were developed to enable system design by describing the interactions of the STDR/SSTDR signal and various types of noise in the correlator output. Simulations were performed for STDR and SSTDR tests for ML codes in the presence of a Mil-Std 1553 background signal to study the effects of this type of noise on STDR/SSTDR tests. Equations were developed to describe the effects of scaling test system parameters including the number of chips in the PN sequence and the PN sequence chip rate used for STDR and SSTDR. It was shown that doubling the PN code length doubles the SNR independent of the noise type, and that doubling the chip rate (and modulation frequency for SSTDR) in the presence of Mil-Std 1553 can have no appreciable effect on the SNR for STDR, but can increase the SNR for SSTDR by 6 dB.

ML codes were identified as the best code to use for testing single wires at a time due to the higher self-induced noise present with other code choices. Kasami codes are the optimal codes to use when performing multiple interacting tests simultaneously.

The work covered in this paper shows that SSTDR and STDR can be effective tools for locating defects on live cables, and this was demonstrated for both controlled and uncontrolled impedance cables carrying 60 Hz (similar to 400 Hz) and 1-MHz Mil Std 1553 signals. This discussion has shown that

STDR and SSTDR are equally suited for testing in the presence of white noise or low frequency signals (such as 60- or 400-Hz power), but that SSTDR is a better choice for testing in the presence of the high-frequency data signals typically found on aircraft cables.

The discussion in this paper suggests that STDR and SSTDR test system parameters could be adjusted so that the test signal levels are below the noise tolerance of other signals on the wires, while still providing a sharp correlation peak to detect changes in impedance along the length of the cables. These features make it feasible to use SSTDR and to a lesser degree STDR to test live wires on aircraft in flight. Because the tests can be performed continuously, intermittent failures such as open circuits, short circuits, and arcs could be detected and recorded when they occur, enabling maintenance personnel on the ground to quickly identify the nature and location of intermittent wiring problems so they can be resolved. Further evaluation of this method for locating intermittent "soft" faults can be found in [18]. Faults with lower impedance, either on a "hot" wire or on the ground return, have less reflection and, therefore, less SNR. Detection of these faults is limited by the SNR required for detection and the noise in the measured correlation.

REFERENCES

- [1] R. Pappas, "Aging systems research program," presented at the DER Recurrent Seminar, Sep. 2000.
- [2] C. Furse and R. Haupt, "Down to the wire," *IEEE Spectrum*, vol. 38, no. 2, pp. 34–39, Feb. 2001.
- [3] S. Field, P. Arnason, and C. Furse, "Smart wire technology for aircraft applications," presented at the 5th Joint NASA/FAA/DoD Conf. Aging Aircraft, Orlando, FL, Sep. 2001.
- [4] P. Smith, "Spread spectrum time domain reflectometry," Ph.D. dissertation, Dept. Elect. Comput. Eng., Utah State Univ., Logan, 2003.
- [5] M. B. Djuric *et al.*, "Digital signal processing algorithms for arcing fault detection and fault distance calculation on transmission lines," *Elect. Power Energy Syst.*, vol. 19, no. 3, pp. 165–170, 1997.
- [6] V. Taylor and M. Faulkner, "Line monitoring and fault location using spread spectrum on power line carrier," *Proc. Inst. Elect. Eng.*, vol. 143, pp. 427–434, Sep. 1996.
- [7] K. Jones *et al.*, "Adaptive method and apparatus for transmission line analysis," U.S. Patent 20020169585, Mar. 11, 2002.
- [8] M. F. Iskander, *Electromagnetic Fields and Waves*. Englewood Cliffs, NJ: Prentice-Hall, 1992.
- [9] Y. Chung, C. Furse, and J. Pruitt, "Application of phase detection frequency domain reflectometry for locating faults in an F-18 flight control harness," *Trans. IEEE Electromagn. Compat.*, vol. 47, no. 2, pp. 327–334, May 2005.
- [10] R. C. Dixon, *Spread Spectrum Systems*. New York, NY: Wiley, 1984.
- [11] J. G. Proakis and M. Salehi, *Communication Systems Engineering*. Englewood Cliffs, NJ: Prentice-Hall, 1994.
- [12] P. J. Medelius and H. J. Simpson, "Non-intrusive impedance-based cable tester," U.S. Patent 5 977 773, Aug. 15, 1997.
- [13] D. Bates, "Wireless communication and signal processing for aging aircraft wiring," M.S. thesis, Dept. Elect. Comput. Eng., Utah State Univ., Logan, 2002.
- [14] K. Shull, L. C. Brinson, N. Nunalee, T. Bai, T. Mason, and S. Carr, "Aging characterization of polymeric insulation in aircraft wiring via impedance spectroscopy," in *Proc. 5th Joint NASA/FAA/DoD Conf. Aging Aircraft*, Sep. 2001, pp. 55–61.
- [15] P. Smith, "Using inert gas to enhance electrical wiring inspection," presented at the 6th Joint FAA/DoD/NASA Conf. Aging Aircraft, San Francisco, CA, Sep. 2002.
- [16] B. Sklar, *Digital Communications, Fundamentals and Applications*. Englewood Cliffs, NJ: Prentice-Hall, 1988.
- [17] *Mil-Std-1553 Designers Guide*, 6th ed. New York: ILC Data Device Corp., 1998, pp. II-28–II-48.
- [18] C. Furse, P. Smith, M. Safavi, and C. Lo, "Feasibility of spread spectrum sensors for location of arcs on live wires," *IEEE Sensors J.*, vol. 5, no. 6, pp. 1445–1450, Dec. 2005.



Paul Smith (M'02) received the M.B.A. degree in 1996 and the Ph.D. degree in 2003.

He is currently the President of LiveWire Test Labs., Inc., Salt Lake City, UT, which builds hardware for locating intermittent wire faults. He has over 11 years of experience designing cable and wire harness test equipment. He has been working on solutions to difficult wire test issues and holds patents, and has patents pending, in the field. He has a background in business management, electronic circuit design, electromechanical system design, electromagnetic theory, nonlinear inversion theory, microwaves, quantum mechanics, and optics.



Cynthia Furse (SM'99) received the Ph.D. degree in 1994.

She is the Director of the Center of Excellence for Smart Sensors, University of Utah, Salt Lake City, where she is also an Associate Professor in the Electrical and Computer Engineering Department. The Center focuses on embedded sensors in complex environments, particularly sensors for anomalies in the human body and aging aircraft wiring. She has directed the Utah "Smart Wiring" program, sponsored by NAVAIR and USAF, since 1997. She teaches electromagnetics, wireless communication, computational electromagnetics, microwave engineering, and antenna design.

Dr. Furse was the 2000 Professor of the Year at the College of Engineering, Utah State University, Logan, the 2002 Faculty Employee of the Year, a National Science Foundation Computational and Information Sciences and Engineering Graduate Fellow, IEEE Microwave Theory and Techniques Graduate Fellow, and Presidents Scholar at the University of Utah. She is the Chair of the IEEE Antennas and Propagation Society Education Committee and an Associate Editor of the IEEE TRANSACTIONS ON ANTENNAS AND PROPAGATION.



Jacob Gunther (M'99) was a Research Assistant with the Microwave Earth Remote Sensing Laboratory, Brigham Young University, Provo, UT, from 1992 to 1994. From 1994 to 1995, he was with Lockheed-Martin, Manassas, VA, where he worked on target detection algorithms, sonar systems, and satellite digital communication systems. From 1998 to 2000, he was with Merasoft, Inc., Provo, where he worked on speech recognition, speaker identification, and noise cancellation using microphone arrays. He joined the faculty of the Department of Electrical and

Computer Engineering department, Utah State University, Logan, in 2000. His research interests include array signal processing for wireless communications, blind deconvolution and source separation, and system identification.